High Performance GPU Bayesian Image Synthesis

Conference Paper · December 2015

DOI: 10.1109/ISSPIT.2015.7394340

5 authors, including:

Miguel Cárcamo
University of Santiago, Chile
3 PUBLICATIONS **0** CITATIONS

SEE PROFILE

Fernando R Rannou
University of Santiago, Chile
39 PUBLICATIONS **1,856** CITATIONS

SEE PROFILE

Pablo Enrique Roman
University of Santiago, Chile
44 PUBLICATIONS **347** CITATIONS

SEE PROFILE

High Performance GPU Bayesian Image Synthesis

Miguel Cárcamo*, Fernando R. Rannou*, Pablo E. Román†, Victor Moral‡ and Simon Casassus‡
*Departamento de Ingeniería Informática, Universidad de Santiago de Chile,
Región Metropolitana, Santiago, CHILE.
E-mail: miguel.carcamo@usach.cl Tel: +56-9-74315582
fernando.rannou@usach.cl Tel: +56-9-82349110
†Center for Mathematical Modeling, Universidad de Chile,
Av. Blanco Encalada 2120 Piso 7, Santiago, CHILE.
E-mail: proman@ing.uchile.cl Tel: +56-2-29784859
‡Astronomy Department, Universidad de Chile,
Camino El Observatorio 1515, Las Condes, Santiago, CHILE.
E-mail: vmoral@das.uchile.cl
scasassus@u.uchile.cl Tel: +56-2-29771137

***Abstract*—ALMA is a revolutionary instrument in its scientific concept, its engineering design and its organisation as a global effort. ALMA and new incoming radio-telescopes delivery big amounts of data that are useful to the sky image reconstruction. In this context, MEM is one of the most recognized reconstruction algorithms in radio-interferometry and is based on a Bayesian approach. Our results show that an GPU implementation of this algorithm on a half of and NVIDIA K80 is approximately 100 to 500 times faster than the multi-core implementation.**

***Keywords*—GPU, ALMA, Fourier Synthesis, CUDA, Radiointerferometry, General Purpose GPU, Imaging, Image Reconstruction.**

I. Introduction

Astronomy researchers have been benefited from recent cutting-edge radio telescope such ALMA[1] which consists of a number of antennas capable of collecting radio signals in the millimeter and sub-millimeter range. Each antenna's signal is correlated with every other signal to produce samples of the sky image, but on the Fourier domain [2]. Typical sampling data set varies from 10^4 to more than 10^7 sparse samples that are used to reconstruct the sky image. The process to solve the inverse problem of recovering the image from a sparse and irregularly sampled Fourier data is called Image Synthesis [3] or Fourier Synthesis [4].

Equation 1 states the simple functional relationship between the image $I(x, y)$ and its associated interferometric signal [5] called the Visibility function $V(u, v)$

$$V(u,v) = \int_{\mathbb{R}^2} A(x,y)I(x,y)e^{-2\pi i(ux+vy)}dxdy \qquad (1)$$

The kernel $A(x, y)$ is called the primary beam (PB) and corresponds to the solid angle reception pattern of the antenna array and modelled as a Gaussian function [6]. For simplicity, in this paper we assume $I(x, y) \equiv A(x, y)I(x, y)$ and with the same support of A. In this case the visibility function is simply the Fourier Transform of the image $V = \mathcal{F}\{I\}$. Current interferometers are able to collect a large number of (observed) samples $\{V_k^o\}_{k=1}^Z$ at spatial frequencies $\{Z_k = (u_k, v_k)\}_{k=1}^Z$ in order to fill as much as possible the Fourier domain. Additionally, the interferometer is able to measure data variance σ_k^2 per visibility as a function of the antenna thermal noise [3].

Many algorithms have been proposed for solving the image synthesis problem and the de-facto standard procedure is the CLEAN heuristic [7]. This algorithm is based on the dirty image/beam representation of the problem [6], which results in a deconvolution problem. CLEAN has been interpreted as a greedy class heuristic, particularly for point-like sources as a matching pursuit algorithm [8]. Image reconstruction in CLEAN can be done in either the image or Fourier space, and it is therefore quite efficiently implemented using FFTs. However, statistical interpretation of resulting images and remaining artifacts are far to be described by a well founded theory. Nevertheless, with the help of additional information like the physics of the observed object, astronomers are able to interpret CLEAN images with certain degree of success.

Image synthesis is an ill-posed problem [4], [9]; it has no unique solution, and it behaves in a non-continuously manner due to variations of its parameters. A common approach for approximating a solution is to introduce a regularization term which reduces the solution space and the number of free parameters to the order of the number of image pixels. The image synthesis problem is then formulated as a non-linear optimization problem.

The maximum entropy algorithm (MEM) [10], [11], [12] is a well known alternative to CLEAN. It is based on a maximum likelihood argumentation since interferometer measurements are corrupted by noise. Reconstructed images with this method have been considered to have higher resolution and less artifacts than CLEAN images. However, routine use of MEM with large data sets has been hindered due to its high computational demands [6], [13].

In this context, we are interested in developing high performance solutions for large scale image synthesis problems and develop a GPU implementation of MEM. Although, multithread (`uvmem`) have been used in astrophysics [14], [15], [16], [17], [18], [19], the algorithm and its implementation details have never been published before. Additionally, the amount of data that ALMA will generate in the near future requires

a massively parallel, high throughput approach, which cannot be delivered by nowadays multi-core computers. Fortunately, GPUs have grown from particular purposes (video games, 3D movies, etc.) to scientific and general purposes applications, allowing scientific community and researchers exploit their computing power with relative ease [20]. Recently, a GPU implementation for solving the Bayesian Inference for Radio Observations [21] has been proposed [22]. This approach uses Bayesian inference to sample a parameter set representing a sky model to propose visibilities that best match the model. Currently, their model handles point and Gaussian sources. Our approach employs a non-linear optimization problem to directly solve the Bayesian model with the maximum entropy prior. We will show the power of GPU computing with several ALMA data sets and compare its computational performance against a multi-thread solution.

This paper is organized as follows. Section II describes the MEM formulation together with its GPU implementation. Section III presents several reconstruction experiments with ALMA data. Section IV establishes the main conclusions and future work.

II. Method and Implementation

This section describes the mathematical formulation of the *Maximum Entropy Method* (MEM) together with a positively constrained conjugate gradient minimization algorithm. Finally, some GPU implementation details are given.

A. Maximum Entropy Method

The deconvolution problem consists of selecting one image from many feasible. MEM is an important class of image restoration algorithm that selects the image that fits with the measured visibilities, to within the noise level, and whose pixel values satisfy the maximum entropy restriction [3], [23].

In MEM, image and data are considered random variables, with known probability distributions. Let $P(V|I)$ the likelihood of seeing the visibilities V given the image I and let $P(I)$ be an *a priori* knowledge of the image. Then, by Bayes theorem we obtain the *a posteriori* probability

$$P(I|V) = \frac{P(V|I)P(I)}{P(V)} \tag{2}$$

The likelihood $P(V|I)$ can be approximated using the fact that visibilities are corrupted by heterocedastics Gaussian noise. Given a model function of visibilities $V_k^m(I)$ and the observed variances σ_k the probability is proportional to the expression (3).

$$P(V|I) \propto \exp\left\{ -\sum_k^Z \left| \frac{V_k^m(I) - V_k^o}{\sigma_k} \right|^2 \right\} \tag{3}$$

The prior $P(I)$ is modeled considering a multinomial distribution of a discrete total intensity that covers the entire image. Let n be the number of image pixels and let N_i be the number of photons collected at pixel i. Then, the prior can be expressed as

$$P(I) = \frac{N!}{n^N \prod_i N_i!} \tag{4}$$

where $N = \sum_i N_i$. The image intensity at pixel i is interpreted in this model as $I_i \propto N_i$.

The term $P(V)$ in equation 2 is independent of I, and therefore we drop it from the equation. Taking logarithm, using the Stirling approximation for factorials, and omitting irrelevant additive constants, the image reconstruction problem becomes finding the image that satisfies the Maximum a Posteriori Probability (MAP), that is:

$$\arg\max_I \left\{ -\frac{1}{2} \sum_k^Z \left| \frac{V_k^m(I) - V_k^o}{\sigma_k} \right|^2 - \lambda \sum_i^n I_i \log \frac{I_i}{G} \right\} \tag{5}$$

We recognize equation 5 as a typical χ^2 term plus a Shannon's entropy term S. Two parameters are relevant in this model, namely λ that has a similar role as a Lagrange multiplier and G that can be interpreted as the background noise.

Finally, we change the sign of equation 5 and turn to a minimization problem, where the objective function is:

$$\Phi = \frac{1}{2} \sum_k^Z |\frac{V_k^m(I) - V_k^o}{\sigma_k}|^2 + \lambda \sum_i^n I_i \log \frac{I_i}{G} \tag{6}$$

B. Multidimensional Conjugate Gradient Method Minimization

The minimization problem is solved by a positively constrained conjugate gradient (CG) algorithm. Specifically, we use a Polak-Ribiere's method [24], [25] modified such that to include the positivity constraint.

The Polak-Ribiere algorithm is given as:

1: Select $I_0 \in \Re^n$
2: $d_0 = -\nabla\Phi(I_0)$
3: **for** i=0 **to** MAX ITERATIONS **do**
4: Compute α_i such that $\Phi(I_i+\alpha_i d_i) = \min_\alpha \Phi(I_i+\alpha_i d_i)$
5: Set $I_{i+1} = I_i + \alpha_i d_i$
6: **if** $||\nabla\Phi(I_{i+1})|| = 0$ **then**
7: Stop.
8: **else**
9: $g_{i+1} = -\nabla\Phi(I_{i+1})$
10: $\beta_i = \frac{g_{i+1}^T(g_{i+1}-d_i)}{d_i^T d_i}$
11: $d_{i+1} = g_{i+1} + \beta_i d_i$
12: **end if**
13: **end for**

Fig. 1. Polak Ribiere's algorithm

At line 1, the algorithm begins with any positive guess of the image, and computes the initial search direction at line 2. It then begins the iteration loop searching for the minimum. To compute the next image, it has to find an α value that minimizes the objective function along the search direction

and subject to the positive constraint (line 4). At line 6, the algorithm checks whether a minimum has been found, in which case it stops. Otherwise, it computes a new search direction using the Polak-Ribiere variant (line 9-11).

C. GPU Implementation

A general CPU/GPU architecture is shown in Figure 2. The system can have many GPUs connected to the CPU or host, but they cannot communicate directly among each other. All synchronization and data communication must be done through the host. Thus, the host is in charge of calling kernels to the various devices available and copying data back and forth between host memory and GPUs memories. As shown in Figure 2, a GPU is built around a small number of Streaming Multiprocessors (SM), which in turn are composed of many Streaming Processors (SP). SP are also called CUDA cores and they are the compute units that execute instructions. Currently, threads that execute in the same SM can communicate through shared memory, but when they reside in different SM they must communicate through the host.

The implementation of the Polak-Ribiere algorithm consists of two main parts, namely the one running in the host and the one running in GPU. The algorithm itself is implemented in host and it is in charge of calling GPU kernels to apply the primary beam to the image, evaluate the objective function, calculate $\nabla\chi^2$ and ∇S, and move data back and forth between host memory and device memory.

For instance, line 4 of algorithm in figure 1 shows the 1D line minimization to calculate the step size α_i. This procedure runs in the host CPU but the actual image update in line 5 is carried out by a 2D grid kernel. Similarly, line 6 shows the computation of the gradient's norm which is also coded in a 2D grid kernel with a sum reduction whose result is moved back to the host.

Notice that the calculation of β_i in line 10 also requires a sum reduction. Here, there are three kernels involved: one for computing the numerator, one for computing the denominator and finally one for carrying out the two sum reductions. After getting the two scalar values, these are moved to host where the final division is computed.

Finally the calculation of the new search direction in line 11 is executed by a kernel which receives as parameters the gradient of the new image $\nabla\Phi(I_{i+1})$, the current search direction, and the β value. Once again, this is done with a 2D grid kernel.

At each iteration, the evaluation of the objective function requires the computation of updated model visibilities. For this we employ NVIDIA's implementation of the FFT (`cuFFT()`) [26], which has best performance when transform sizes are powers of a single factor. This is why we prefer to work with images whose sizes are power of 2.

Figure 3 summarizes the image reconstruction process, which starts with a uniform image I stored in a bidimensional array. The 2D FFT applied to the image returns complex values located on a regular grid, which must be interpolated to obtain model visibilities V^m at the non-regularly sampled spatial frequencies Z_k. Then, Φ and $\nabla\Phi$ are computed as before above, and these are used by the Polak-Ribiere algorithm to

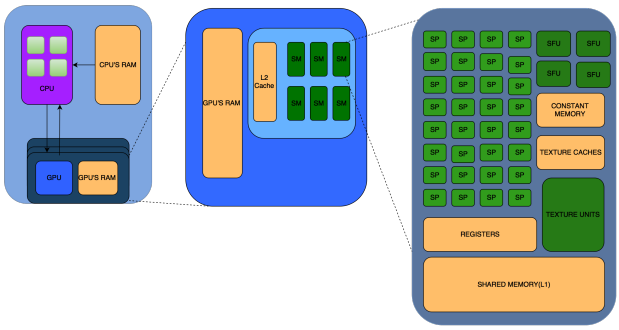

Fig. 2. GPU Architecture.

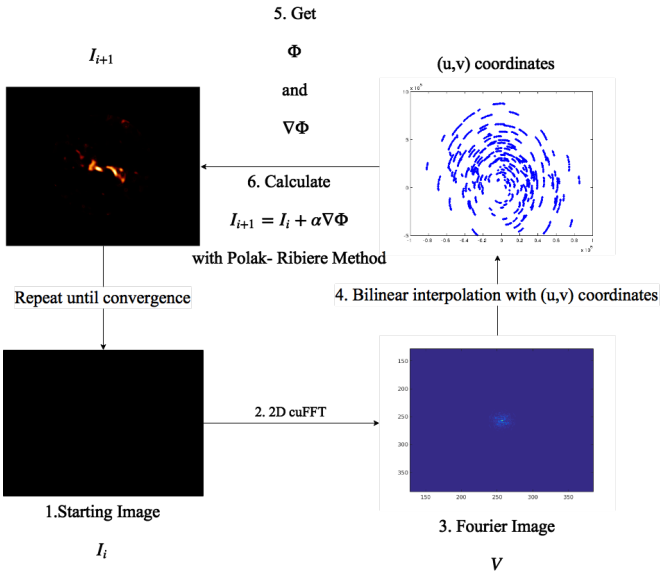

Fig. 3. Image Reconstruction Process.

generate a new image estimate. The process is repeated until convergence is achieved or the maximum number of iterations is reached.

III. Experimental Results

A. Materials and methods

Two real ALMA data sets were used in our experiments. The first one corresponds to the CO(6-5) ALMA dataset on band 9 that has a total of 120982 visibilities with two Stokes polarization (XX, YY). This corresponds to the emission line of carbon monoxide in the proto-planetary disk HD142527 [27]. The second data set is the proto-planetary disk HD142527, on band 9 continuum spectral on 709GHz. This data set (code: ADS/JAO.ALMA#2011.0.00465.S) has 78375 visibilities with two Stokes polarization (XX,YY). The observed object corresponds to a young star localized at 140 Pc from earth, and surrounded by gas and dust orbiting around. Its continuum emission has an asymmetrical shape similar to a horseshoe [28].

The GPU implementation was run in a GK210 (a half of a K80 NVIDIA Tesla card) with a Kepler architecture, 2496

streaming processors (CUDA cores) and 12 Gbytes of global memory. Since the fastest version of MEM we currently have is a multithreaded version, we also include execution time of our GPU implementation against this multi-core version on a 2x 10 Core Intel Xeon E5-2640 V2 2GHz processor. Although, these two architectures are not comparable the speedup gained using GPUs show users (astronomers) the potential that this tool can have for image reconstruction in production mode.

B. *Computational performance*

Tables I and II show execution times and speedup results for the two data set and for several image sizes. It is important to emphasize that execution time depends not only on known factors like image size and number of visibilities, but also on the number of iterations the algorithm needs to converge to a solution. In any case, best speedups are achieved for the largest image size. Notice how GPU execution time increases more slowly than the CPU time as the image size is increased. For instance, in Table I when doubling the image size from 256×256 to 512×512 pixels, the GPU time increases from 11.87 seconds to only 13.13 seconds, but the CPU time increases from 189 to 1127 seconds.

It is also worth noticing how the second data set reconstruction takes more time than the first data set, even though the later one has 40 thousand more visibilities. This is due to the fact that CO(6-5) contain visibilities on only one frequency, but HD142527 in three. This leads to a lost of throughput in the HD142527 execution, because the process of calculating Φ and $\nabla\Phi$ has to be done separately each time for each frequency, and then sum up the results.

TABLE I. CO(6-5) PERFORMANCE

Image Size	Time (s)		Speedup
	CPU	GPU	
128x128	49	2.79	17.56
256x256	189	11.87	15.92
512x512	1127	13.13	85.83
1024x1024	6721	18.55	524.04

TABLE II. HD142527 PERFORMANCE

Image Size	Time (s)		Speedup
	CPU	GPU	
128x128	212	5.5	38.5
256x256	477	14.7	32.4
512x512	3007	35.1	85.7
1024x1024	4818	47.6	101.2

Although in this paper we do not compare and evaluate image quality, we show images reconstructed with CLEAN and MEM.

Figures 4 and 5 display the result for CO(6-5) and figures 6 and 7 for HD142527. The entropy penalty factor for CO(6-5) and HD142527 were 0.2 and 0.001, respectively.

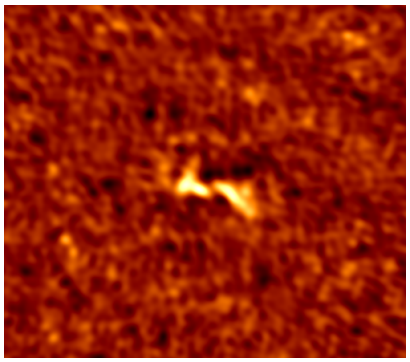

Fig. 4. CO(6-5) CLEAN Image.

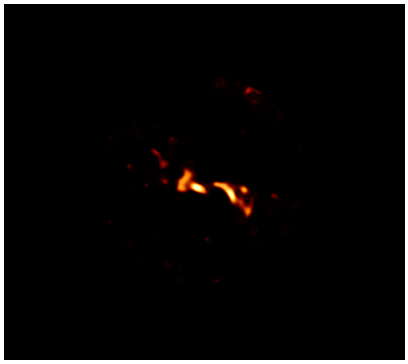

Fig. 5. CO(6-5) MEM Image.

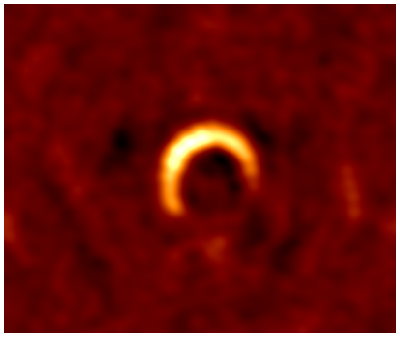

Fig. 6. HD142527 CLEAN Image.

Fig. 7. HD142527 MEM Image.

IV. CONCLUSION

In this paper we have shown that it is possible to reconstruct ALMA images with a high-performance GPU implementation of MEM. Computational results indicate that our GPU implementation can reconstruct images 524 times faster than an equivalent 20 core multi-thread solution. More importantly,

GPU appears to be highly scalable as reconstruction times grow slowly with respect to image size and number of visibilities. This is highly relevant, since ALMA and the new radiotelescope SKA [29] will generate bigger amounts of data. In this context, future work involves a harnessing the power of Tesla K80 and use a multiple GPU approach to distribute data and computation.

ACKNOWLEDGMENT

This paper makes use of the following ALMA data: ADS/JAO.ALMA#2011.0.00465.S. ALMA is a partnership of the ESO, NSF, NINS, NRC, NSC and ASIAA. The Joint ALMA Observatory is operated by the ESO, AUI/NRAO and NAOJ. PR acknowledge Fondecyt 3140634.

REFERENCES

[1] A. B. Peck and A. J. Beasley, "High resolution sub-millimeter imaging with ALMA," *Journal of Physics: Conference Series*, vol. 131, no. 1, p. 012049, 2008. [Online]. Available: http://stacks.iop.org/1742-6596/131/i=1/a=012049

[2] C. Candan, M. Kutay, and H. Ozaktas, "The discrete fractional fourier transform," *Signal Processing, IEEE Transactions on*, vol. 48, no. 5, pp. 1329–1337, May 2000.

[3] G. A. Richard Thompson, James M. Moran, *Interferometry and Synthesis in Radio Astronomy*. Weinheim: WILEY-VCH Verlag GmbH & Co. KGaA, 2004.

[4] P. Marchal and D. Wallach, "Fourier synthesis via partially finite convex programming," *Mathematical and Computer Modelling*, vol. 49, no. 1112, pp. 2206 – 2212, 2009, trends in Application of Mathematics to MedicineTrends in Application of Mathematics to Medicine. [Online]. Available: http://www.sciencedirect.com/science/article/pii/S0895717708002380

[5] B. G. Clark, "Coherence in Radio Astronomy," in *ASP Conf. Ser. 180: Synthesis Imaging in Radio Astronomy II*, G. B. Taylor, C. L. Carilli, and R. A. Perley, Eds., 1999, pp. 1+. [Online]. Available: http://adsabs.harvard.edu/cgi-bin/nph-bib_query?bibcode=1999ASPC..180....1C

[6] G. B. Taylor, C. L. Carilli, and R. A. Perley, Eds., *Synthesis Imaging in Radio Astronomy II*, ser. Astronomical Society of the Pacific Conference Series. San Francisco: Astronomical Society of the Pacific, 1999, vol. 180. [Online]. Available: http://adsabs.harvard.edu/cgi-bin/nph-bib_query?bibcode=1999ASPC..180.....T

[7] J. A. Hogbom, "Aperture Synthesis with a Non-Regular Distribution of Interferometer Baselines," *Astron. Astrophys. Suppl. Ser.*, vol. 15, pp. 417–426, 1974.

[8] A. Lannes, E. Anterrieu, and P. Marechal, "Clean and Wipe," , vol. 123, pp. 183–198, May 1997.

[9] W. Chen, "The ill-posedness of the sampling problem and regularized sampling algorithm," *Digital Signal Processing*, vol. 21, no. 2, pp. 375 – 390, 2011. [Online]. Available: http://www.sciencedirect.com/science/article/pii/S1051200410001454

[10] T. J. Cornwell and K. F. Evans, "A simple maximum entropy deconvolution algorithm," , vol. 143, pp. 77–83, Feb. 1985.

[11] J. G. Ables, "Maximum Entropy Spectral Analysis," , vol. 15, p. 383, Jun. 1974.

[12] S. F. Gull and G. J. Daniell, "Image reconstruction from incomplete and noisy data," *Nature*, vol. 272, no. 5655, pp. 686–690, Apr. 1978. [Online]. Available: http://dx.doi.org/10.1038/272686a0

[13] R. Narayan and R. Nityananda, "Maximum entropy image restoration in astronomy," , vol. 24, pp. 127–170, 1986.

[14] S. Perez, S. Casassus, F. Menard, P. Roman, G. van der Plas, L. Cieza, C. Pinte, V. Christiaens, and A. S. Hales, "Co gas inside the protoplanetary disk cavity in hd 142527: Disk structure from alma," *The Astrophysical Journal*, vol. 798, no. 2, p. 85, 2015.

[15] H. Canovas, M. R. Schreiber, C. Caceres, F. Menard, C. Pinte, G. S. Mathews, L. Cieza, S. Casassus, A. Hales, J. P. Williams, P. Roman, and A. Hardy, "Gas inside the 97 au cavity around the transition disk sz 91," *The Astrophysical Journal*, vol. 805, no. 1, p. 21, 2015.

[16] S. Marino, S. Casassus, S. Perez, W. Lyra, P. E. Roman, H. Avenhaus, C. M. Wright, and S. T. Maddison, "Compact dust concentration in the mwc 758 protoplanetary disk," *The Astrophysical Journal*, vol. 0, no. 0, p. 10, 2015, arXiv:1505.06732 [astro-ph.EP], Submitted to.

[17] S. Perez, A. Dunhill, S. Casassus, P. Roman, J. Szulgyi, C. Flores, S. Marino, and M. Montesinos, "Planet formation signposts: observability of circumplanetary disks via gas kinematics," *The Astrophysical Journal*, vol. 0, no. 0, p. 10, 2015, arXiv:1505.06808 [astro-ph.EP], Submitted to.

[18] S. Casassus, S. Marino, S. Perez, P. Roman, A. Dunhill, P. Armitage, J. Cuadra, A. Wootten, G. van der Plas, L. Cieza, V. Moral, V. Christiaens, and M. Montesinos, "Accretion kinematics through the warped transition disk in hd142527 from resolved co(6-5) observations," *The Astrophysical Journal*, vol. 0, no. 0, p. 10, 2015, arXiv:1505.07732 [astro-ph.SR], Submitted to.

[19] S. Casassus, C. Wright, S. Marino, S. T. Maddison, A. Wootten, P. Roman, S. Perez, P. Pinilla, M. Wyatt, V. Moral, F. Menard, V. Christiaens, L. Cieza, and G. van der Plas, "A compact concentration of large grains in the hd142527 protoplanetary dust trap," *The Astrophysical Journal*, vol. 0, no. 0, p. 10, 2015, arXiv:1505.07743 [astro-ph.SR], Submitted to.

[20] J. D. Owens, D. Luebke, N. Govindaraju, M. Harris, J. Krger, A. Lefohn, and T. J. Purcell, "A survey of general-purpose computation on graphics hardware," *Computer Graphics Forum*, vol. 26, no. 1, pp. 80–113, 2007. [Online]. Available: http://www.blackwell-synergy.com/doi/pdf/10.1111/j.1467-8659.2007.01012.x

[21] M. Lochner, I. Natarajan, J. T. L. Zwart, O. Smirnov, B. A. Bassett, N. Oozeer, and M. Kunz, "Bayesian inference for radio observations," , vol. 450, pp. 1308–1319, Jun. 2015.

[22] S. Perkins, P. Marais, J. Zwart, I. Natarajan, and O. Smirnov, "Montblanc: GPU accelerated radio interferometer measurement equations in support of bayesian inference for radio observations," *CoRR*, vol. abs/1501.07719, 2015. [Online]. Available: http://arxiv.org/abs/1501.07719

[23] T. J. Cornwell, "Radio-interferometric imaging of very large objects," , vol. 202, pp. 316–321, Aug. 1988.

[24] W. H. Press, S. A. Teukolsky, W. T. Vetterling, and B. P. Flannery, *Numerical Recipes in C (2Nd Ed.): The Art of Scientific Computing*. New York, NY, USA: Cambridge University Press, 1992.

[25] E. Polak and G. Ribiere, "Note sur la convergence de mthodes de directions conjugues," *ESAIM: Mathematical Modelling and Numerical Analysis - Modlisation Mathmatique et Analyse Numrique*, pp. 35–43, 1969.

[26] NVIDIA Corporation, *CUDA Toolkit 5.0 CUFFT Library Progrraming Guide*. NVIDIA Corporation, 2012, version 0.1.

[27] S. Casassus, S. Marino, S. Prez, P. Roman, A. Dunhill, P. J. Armitage, J. Cuadra, A. Wootten, G. van der Plas, L. Cieza, V. Moral, V. Christiaens, and M. Montesinos, "Accretion kinematics through the warped transition disk in hd142527 from resolved co(65) observations," *The Astrophysical Journal*, vol. 811, no. 2, p. 92, 2015. [Online]. Available: http://stacks.iop.org/0004-637X/811/i=2/a=92

[28] S. Casassus, G. van der Plas, M, S. P., W. R. F. Dent, E. Fomalont, J. Hagelberg, A. Hales, A. Jordán, D. Mawet, F. Ménard, A. Wootten, D. Wilner, A. M. Hughes, M. R. Schreiber, J. H. Girard, B. Ercolano, H. Canovas, P. E. Román, and V. Salinas, "Flows of gas through a protoplanetary gap," *Nature*, vol. 493, pp. 191–194, Jan. 2013.

[29] P. Quinn, T. Axelrod, I. Bird, R. Dodson, A. Szalay, and A. Wicenec, "Delivering SKA science," *CoRR*, vol. abs/1501.05367, 2015. [Online]. Available: http://arxiv.org/abs/1501.05367